Interfacial Behavior of Block Polyelectrolytes. 5. Effect of Varying Block Lengths on the Properties of Surface Micelles

J. Zhu, A. Eisenberg,* and R. B. Lennox*

Department of Chemistry, McGill University, 801 Sherbrooke Street West, Montreal, Quebec, Canada H3A 2K6

Received December 26, 1991; Revised Manuscript Received June 11, 1992

ABSTRACT: Block polyelectrolytes P(S_m-*b*-$VP_n/C_{10}I$) composed of polystyrene blocks (m = 54–480) and perdecylated poly(4-vinylpyridine) (n = 3–240) have been studied using the Langmuir film balance technique and the corresponding Langmuir–Blodgett films. The recently reported phenomenon of surface micelle formation[1] has been found to be very general for those types of materials. Different morphologies, as visualized by transmission electron microscopy, arise, depending on the diblock composition. An unusual phase transition originates from one of the morphological units, i.e., small, circular starfish micelles, and is consistent with an ionic chain solubilization process induced by film compression. As the relative ionic block length is decreased, other morphologies are observed. The properties of surface rod aggregates are consistent with the rods being made up of two layers of the diblocks, with the PS blocks forming the core. Large planar aggregates also form, and appear to be one PS block thick and can extend up to several microns in width. Compressional hysteresis, temperature effects, and aggregation numbers have been used to provide a self-consistent description of the surface micellization phenomenon.

Introduction

The self-assembly of molecules is of central importance in biological organizational states and is the subject of considerable interest in biomimetic studies. Amphiphilic molecules (soaps, detergents, lipids, etc.) are the prototypical self-assembling molecules, and to some extent the factors which govern their organized aggregation have been delineated. These factors, which include van der Waals interactions, hydrogen bonding, electrostatic interactions, and steric interactions, are experimentally accessible using detailed structure/activity studies.[2] More complex self-assembling molecules such as proteins and nucleic acids are also amenable to study using this approach, and, indeed, intermolecular interactions leading to unique self-assembled morphologies can play determining roles in their function.

Recently, block copolymers have been extensively studied in regards to their phase separation behavior and self-assembly capabilities.[3-5] These copolymers, composed of one type block attached to one or two of another type blocks, are interfacially active and can act as compatibilizing agents for two phase-separated materials.[4] Similar behavior has been observed for block ionomers, and their solid-state and solution-based morphologies have also been studied recently.[6]

We have recently undertaken a detailed study of the interfacial properties of AB diblock polyelectrolytes using the Langmuir film balance experiment, where the A block is hydrophobic (i.e., polystyrene) and the B block is hydrophilic (i.e., perquaternized poly(vinylpyridine)).[1,7-9] Although the interfacial properties of low molecular weight (MW) amphiphiles have been extensively studied using the Langmuir film balance experiment,[10] block copolymers have been relatively little studied.[11] We have found that polystyrene-*b*-poly(decylated vinylpyridinium iodide) (P(S_m-*b*-VP_n/C_{10})) unimers spontaneously self-assemble at the air–water interface to form novel aggregates, which we have termed *surface micelles*.[1] These aggregates, visualized as Langmuir–Blodgett films by transmission electron microscopy (TEM) and atomic force microscopy (AFM), assume three forms depending on the block polyelectrolyte composition. When the % PS < 85%, very uniform, circular aggregates form with a hydrophobic core (polystyrene) of diameter ~30–50 nm. Radiating equatorially from this core are the polar vinylpyridinium chains. Rod-shaped aggregates with cross-sectional diameter of ~50–65 nm arise when the PS composition lies between 86% and 94%. Much larger aggregates, ranging from 100 to 7000 nm in diameter when they adopt a circular morphology, arise when the percent composition of PS > 94% in the block polyelectrolyte.[9] Recently, we have also observed the same type of aggregation behavior in nonionic diblocks composed of a highly hydrophobic segment (i.e., PS) and a surface-adsorbed block (i.e., poly(n-butyl methacrylate), poly(dimethylsiloxane)).[12]

Recently, Regen and co-workers[13] and Shen and co-workers[14] have described the film properties of some interesting molecules related to those discussed here. In the former case, calixarene rings substituted with a long polyether chain at each carbon ("octopus" molecules) are found to have compression-induced conformational changes. In our terminology, these small molecules probably undergo a "starfish" → "jellyfish" transition and can be considered to be unimolecular surface micelle analogues. In the latter work, starburst polymers are rendered hydrophilic in the corona via poly(methyacrylic acid) grafts and are spread at the air–water interface. These materials can be viewed as unimolecular polymer analogues to the block polyelectrolyte micelles described in this work.

In this and a companion paper[15] we present a detailed structure/property assessment of PS–PVP block polyelectrolytes and establish the criteria for interfacial self-assembly of these materials. The effect of varying both the absolute and relative sizes of the two blocks while keeping the quaternization agent constant (n-C_{10}) is presented here. Langmuir–Blodgett transmission electron micrographs, Langmuir film surface pressure (π) vs area (A) curves, and the effect of temperature on film properties are combined to provide a detailed insight into the structure of the surface aggregates and their compression-induced structural rearrangements.[1]

Experimental Section

Materials. Synthesis of the P(S_m-*b*-VP_n) diblock copolymers has been previously described in detail.[1] In brief, these materials

* Authors to whom correspondence can be addressed.

0024-9297/92/2225-6547$03.00/0

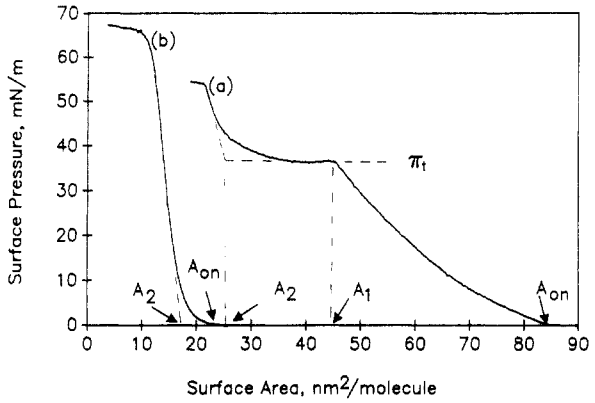

Figure 1. Representation of isotherm parameters in surface pressure vs molecular area (π–A) curves for (a) an isotherm exhibiting a plateau and (b) an isotherm exhibiting only a monotonic increase in surface pressure. π_t is the surface pressure at which the phase transition begins.

were synthesized by sequential anionic polymerization. *n*-Butyllithium was the initiator, and the reaction was carried out in THF at –68 °C. The products were obtained by precipitation in petroleum ether and were dried in a vacuum oven at 70 °C for 72 h. In this study, four different PS blocks were prepared with repeat lengths of 54, 180, 260, and 480 units. The molecular weight of the PS blocks was determined by GPC (Varian; polydispersity = 1.1, 1.2, 1.3, and 1.1 for the $(PS)_{54}$, $(PS)_{180}$, $(PS)_{260}$, and $(PS)_{480}$ samples, respectively), and the VP content was determined by ^1H NMR (200 MHz) and FT-infrared spectroscopy (Analect). Each PS block has attached to it a PVP block, whose VP mole percent varies from 3% to 52%. Poly(4-vinylpyridine) blocks were quaternized using decyl iodide by refluxing in THF (under an N_2 blanket) for 1 week. The extent of quaternization was monitored using FT-IR via the disappearance of the VP absorbance at 1414 cm^{-1}; ~100% quaternization was estimated in each case. In all, 17 P(S-*b*-VP_n/C_{10}) diblock polyelectrolytes were synthesized and characterized using the film balance technique.

Poly(4-vinylpyridine) homopolymer (Polymer Laboratories) having an average MW of 50×10^3 (480 residues per chain) were perdecylated in dry DMF (refluxing under N_2) and was precipitated in acetone. The resulting material is designated P(VP_{480}/C_{10}I).

Surface Balance Measurements. Polymer monolayers were formed at the air–water interface using 0.5 mg/mL stock solutions of polymer dissolved in a 4:1 chloroform/2-propanol solvent. The aqueous subphase was purified and deionized using a Millipore Milli-Q system (18 MΩ) equipped with an organic removal cartridge. The temperature of the subphase was maintained using a Haake circulating-water bath. The surface pressure isotherms were measured using a Langmuir film balance (Lauda Model D).

In a typical experiment, 100 μL of polymer-containing solution was spread on the water surface by depositing ca. 20 5-μL (Hamilton syringe) drops across the entire surface. After waiting 15 min for solvent evaporation, compression was initiated. A number of dynamic parameters were measured, including delay time between deposition and compression, compression rate, and compression–expansion cycling.

The experimental isotherm parameters A_{on}, A_1, A_2, and π_t in surface pressure vs surface area (π–A) curves are as shown in Figure 1. ΔA_t is defined as $(A_2 - A_1)$.

Langmuir–Blodgett (LB) Films and Electron Microscopy. LB films were deposited on an evaporated carbon surface which was in turn supported by a Formvar/EM grid/plastic coverslip sandwich.[1] Y-type films were formed while the surface pressure (2 mN/m) was maintained at a constant value. Dipping speeds were typically 1 mm/min. The air-dried films were shadowed with Pt/Pd (60/40) in a Philips E600 vacuum coater at a shadowing angle of 15–25°. TEM's were obtained with a JEOL CX100-TEMSCAN electron microscope operated at 100 kV. Features observed in the electron micrographs are highly reproducible from sample to sample and are very consistent over the entire coated area (ca. 0.05 cm^2).

Results

Diblock Composition. A series of isotherms obtained at 25 °C on pure water for materials containing different combinations of PS and PVP lengths is shown in Figure 2. In each case, the PVP is perdecylated and is spread on the water surface as the iodide salt. Despite the substantial differences in the length of the PS block (i.e., m = 480 vs 54), considerable similarities in isotherm behavior are evident. For each PS block size, there are corresponding P(VP/C_{10}) block sizes for which a phase transition at high surface pressure is observable. This phase transition is sharp and appears to be first order in nature. The transition pressure, π_t, is found over a limited range (29–38 mN/m) and is highly reproducible from sample to sample under controlled experimental conditions (constant subphase, compression rate, temperature). When the mole fraction of VP/C_{10}I in the diblock is small (<14%), a phase transition does not occur and the π-A curve is smoothly monotonic. This is direct evidence that substantial surface isotherm–MW dependencies arise with these materials.

In all samples presented here (with or without a phase transition) the monolayer becomes highly incompressible at areas <40 nm^2/molecule and it exhibits collapse at high surface pressures (>50 mN/m). Also notable is the observation that the onset of surface pressure (A_{on}) is clearly related to the length of the VP chain, where, for example, A_{on} for P(S_{180}-*b*-VP_{190}/C_{10}I) is 84 nm^2/molecule but for P(S_{180}-*b*-VP_{73}/C_{10}I) it is reduced to 34 nm^2/molecule. The non-PS-containing material, P(S_0-*b*-VP_{480}/C_{10}I) produces a surface film whose isotherm resembles that of the diblocks which have % PS composition <86% except that the transition is marked by a sloped rather than a flat plateau.

Temperature Dependence. A comparison of isotherms acquired at different temperatures provides an insight into the nature of monolayer phase transitions.[16–18] Figure 3 shows the effect temperature has on P(S_{260}-*b*-VP_{120}/C_{10}I) in the experimentally accessible temperature range (5–35 °C). This behavior is qualitatively similar to that reported previously for P(S_{260}-*b*-VP_{240}/C_{10}I).[1] In both cases the plateau pressure, π_t, exhibits an unusual "inversion", where it increases with decreasing temperature. In the case of P(S_{260}-*b*-VP_{120}/C_{10}I), $d\pi_t/dT$ = –0.55 $mN \cdot m^{-1} \cdot K^{-1}$ compared with a $d\pi_t/dT$ = –0.82 $mN \cdot m^{-1} \cdot K^{-1}$ for P(S_{260}-*b*-VP_{240}/C_{10}I).[1]

Kinetic Effects and Hysteresis Phenomena. Of concern in all measurements of monolayers at an air–water interface is whether true equilibrium conditions are attained or whether kinetic effects are coincidentally measured. The question of kinetic factors can be addressed to a certain extent by varying both the compression delay time (time between deposition of the dissolved polymer onto the surface and the time at which compression is initiated) and the actual rate of compression. No quantitative differences in the isotherms were observed for delay times ≥ 15 min; 15 min was therefore used throughout all remaining experiments. The total compression time (t_c) does, however, affect the isotherms. Decreasing the compression rate causes a concomitant decrease in π_t (Figure 4). While a detailed analysis of these kinetics is beyond the scope of our present discussion, Figure 4 clearly shows that even for materials which have flat plateaus, kinetic-dependent processes are clearly being measured at the same time.

While the features of the isotherms remain, for the most part, similar for 30-, 300-, or 600-min total compression times, the details do differ somewhat. For example, the films are more expanded when compressed slowly (A_{on} =

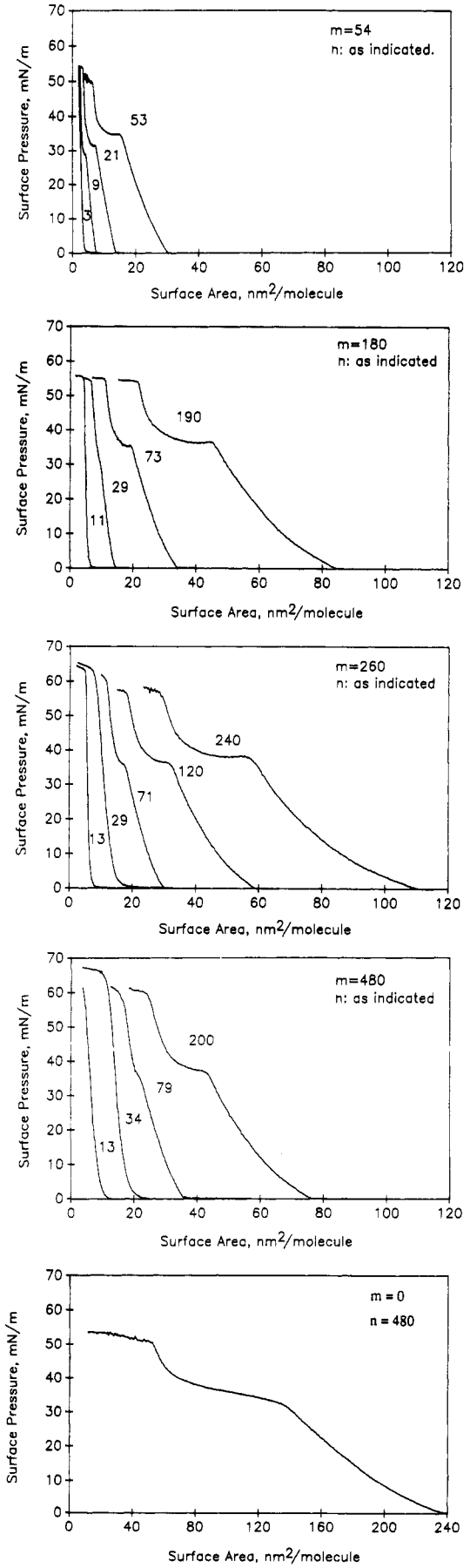

Figure 2. π–A curves for P(S_m-*b*-VP_n/C_{10}I) block polyelectrolytes on a pure water surface at 25 °C, where m is the PS block size and n is the P(VP/C_{10}I) block size. The numbers assigned to each isotherm relate to the P(VP/C_{10}I) block size, n.

132 nm^2/molecule for t_c = 600 min vs 109 nm^2/molecule for t_c = 30 min), have a lower π_t (30 vs 38 mN/m), have a broader ΔA_t (33 vs 22 nm^2/molecule), but have similar A_2 values. The direction of the π_t and ΔA_t changes offset one another in the calculation of ΔH_t and ΔS_t, leading to similar calculated values for ΔH_t and ΔS_t (Table I). Most importantly, both ΔH_t and ΔS_t remain substantially positive in both cases. It is worth noting that another transition is observed at high surface pressures (~45–50 mN/m) during slow compressions. The origin of this transition is currently being studied. These compression rate data establish that the block polyelectrolyte films studied with a 30-min compression regime are not at equilibrium. The trends in film parameters obtained under these conditions do, however, parallel those obtained under conditions closer to equilibrium. Given this and the limitations of both instrumental stability and experimental practicalities, relatively speedy compression rates were used to study these materials.

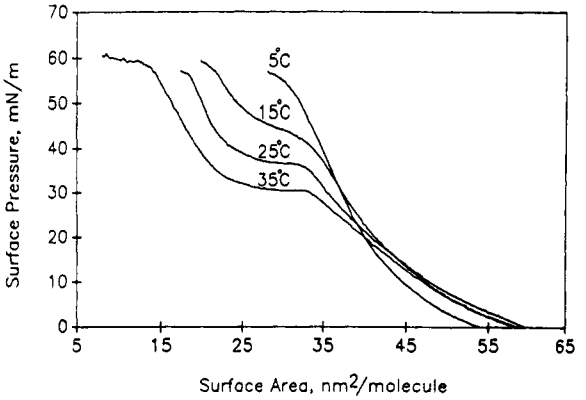

Figure 3. π–A curves of P(S_{260}-*b*-VP_{120}/C_{10}I) at different temperatures on a pure water surface.

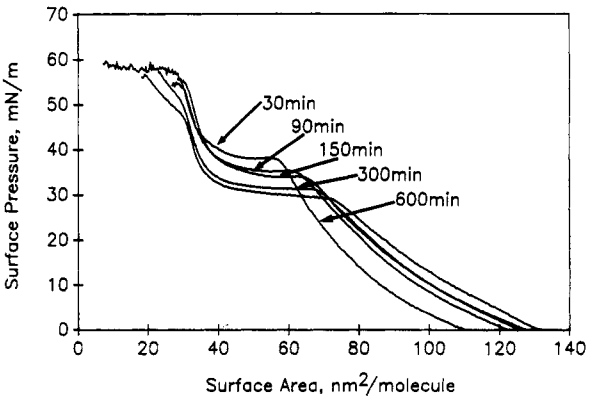

Figure 4. Effect of varying the compression rate for P(S_{260}-*b*-VP_n/C_{10}I) at 25 °C. Time, t_c, refer to the length of time to effect compression of the entire film.

Table I
Calculated ΔS_t and ΔH_t Values for P(S_{260}-*b*-VP_{240}/C_{10}I)

t_c (min)[a]	$d\pi_t/dT$ (mN·m^{-1}·K^{-1})	ΔS_t (eu)[b,c]	ΔH_t (kcal/mol)[b,c]
30	−0.82	8.8	2.6
300	−0.77	11.8	3.5
600	−0.74	11.9	3.5

[a] t_c = time to compress 50 μg of polymer from an area of 928 cm^2 to 27 cm^2. [b] Values are per VP residue. [c] Calculated using the corrected form of the two-dimensional Clausius–Clapeyron equation (ref 17), where $d\gamma°/dT$ = −0.14 mN·m^{-1}·K^{-1} (ref 33).

Compression/expansion experiments of the polymer films shed further light on kinetic effects. As shown in Figure 5, the extent of isotherm hysteresis is strongly dependent upon the area at which the film expansion is initiated. If expansion begins prior to A_1 being achieved, then virtually no hysteresis occurs. If compression goes

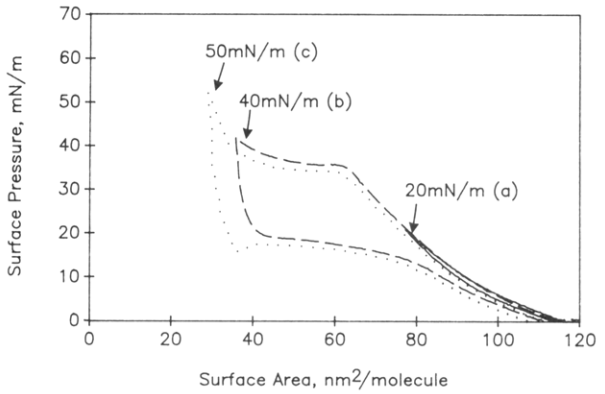

Figure 5. Effect of the surface pressure value at which film expansion is initiated. (a), (b), and (c) represent the first, second, and third compressions of the same film. The π value at which expansion begins is noted wityh each isotherm.

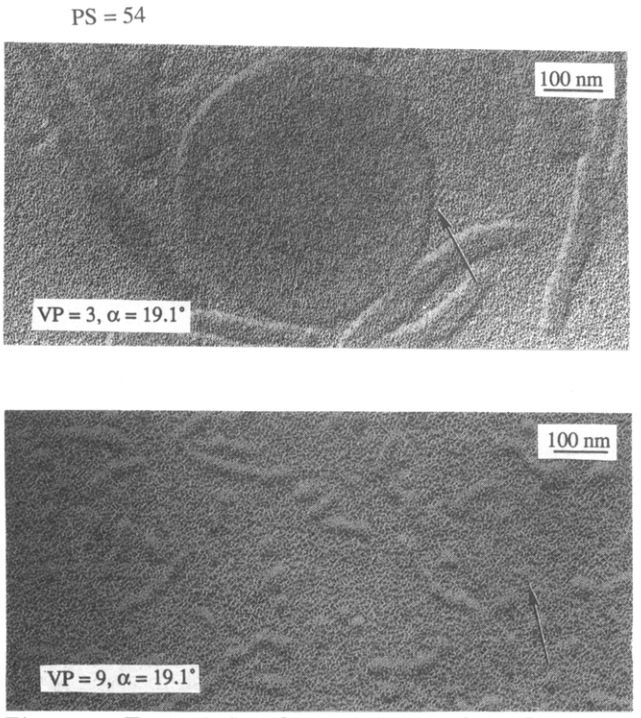

Figure 6. Transmission electron micrographs of Langmuir–Blodgett (LB) films for P(S_m-*b*-VP_n/C_{10}I) shadowed with Pt/Pd (60/40) at a shadowing angle α. The direction of the shadowing is indicated by the arrow in each photograph. Each LB film has been removed from a pure water surface at 2 mN/m onto a Cu grid/Formvar/carbon coated surface. m = 54; n and α are as indicated.

beyond A_1, however, then large hysteresis is observed. With the Langmuir type of film balance used here, it is difficult to determine exactly what is being measured on expansion if the film does not expand homogeneously. Qualitatively, it is apparent that the compressed film expands at a slower rate than the rate of area increase if π_t is reached or exceeded. This effect is a good indication that the highly compressed film has undergone some rearrangement process whose kinetic barrier to return to the initial state conformation is rather large. We have also observed that a film (at 25 °C) taken through a compression/expansion cycle will, if recompressed immediately, exhibit a compression isotherm superimposible on the returning portion of the prior expansion curve.

Langmuir–Blodgett Films. Langmuir–Blodgett films of the block polyelectrolytes shadowed with Pt/Pd (60/40) are readily visualized using transmission electron microscopy[1] or atomic force microscopy.[8] As a handle on

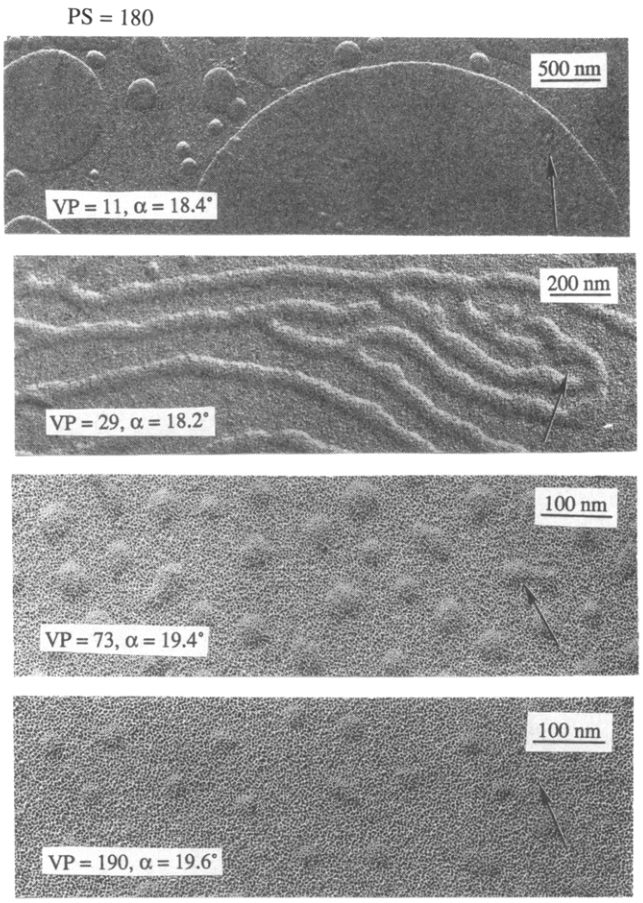

Figure 7. See caption to Figure 6. m = 180; n and α are as indicated.

the morphology of the polymer self-association process, both microscopy techniques are very useful. Shadowed TEM's of representative samples studied as Langmuir–Blodgett films are shown in Figures 6–9. An obvious correlation between isotherms and TEM's can be made—where each sample exhibiting a significant plateau in the isotherm also exhibits an array of highly uniform, circular structures in its LB film. In samples where no plateau is observed in the isotherm, the LB film is primarily made up of either rodlike structures or a polydisperse array of very large, planar circular structures. Recently[9] we have shown that each of these morphologies corresponds to a particular % PS composition range. Small circular structures (i.e., starfish) are found when % PS is < 86%, rods when 86% < % PS < 94%, and large planar aggregates when % PS > 94%. These three different morphologies have corresponding counterparts to the three major morphologies observed in solid-state block copolymers, albeit in very different composition ranges.[19]

The TEM's provide access to the aggregation numbers of the surface micelles. Using a recently presented methodology for determining aggregation numbers in starfish surface micelles,[7] we can determine N_{Agg} from Figures 6–9 and related TEM's. In those cases where the surface micelles are not starfish-like, then only one or two of the five calculation methods[7] can be employed to estimate normalized unimer densities (i.e., the PS area method and the PS volume method). Values of N_{Agg} are listed in Table II for a number of samples visualized as LB films removed at π = 2 mN/m.

Discussion

The air–water monolayers formed by spreading P(S_m-*b*-VP_n/C_{10}I) on pure water reveal distinct block length

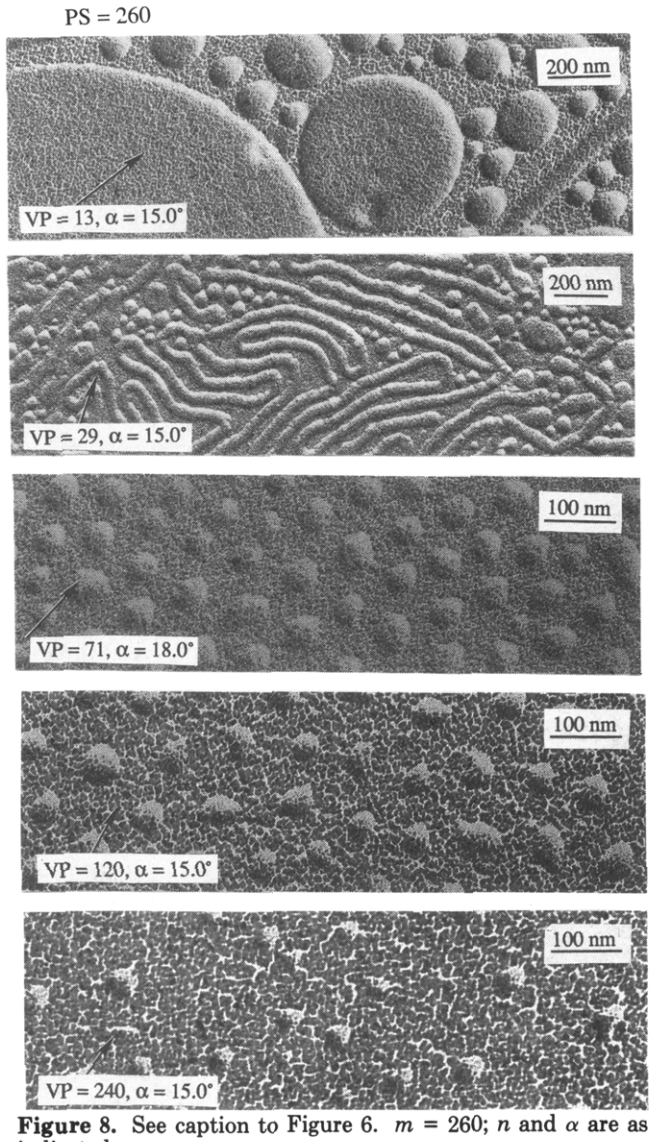

Figure 8. See caption to Figure 6. m = 260; n and α are as indicated.

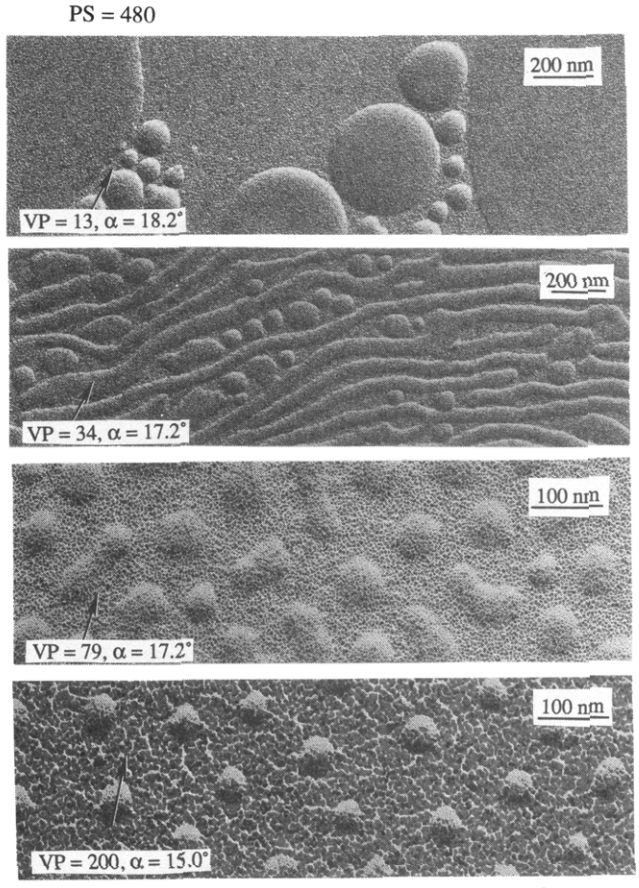

Figure 9. See caption to Figure 6. m = 480; n and α are as indicated.

dependences in both their π–A curve and their LB films. Most dramatic is the association between the presence of a plateau at relatively high surface pressures (i.e., >29 mN/m) and the predominance of small circular aggregates/micelles in the corresponding LB films. Conversely, materials exhibiting no plateau aggregate to form rod or extended planar structures. We therefore conclude that the horizontal region in the π–A curve originates from properties of circular micelles (i.e., starfish) but not rod or planar aggregates (Figure 10). Because of this clear distinction, the following discussion is divided between properties of starfish micelles and rod/planar micelles.

Starfish Micelles. The area at which surface pressure is first noted (A_{on}) is dependent upon the number of VP^+-C_{10} units, n, in a regular fashion for materials shown by TEM to form starfish micelles. A_{on} is proportional to n (r = 0.981) with a proportionality constant of 0.40 nm²/VP residue. An area per VP residue of ≈ 0.40 nm² is slightly less than that estimated from molecular models (0.48 nm², ref 20) for a flat, n-alkylated VP whose decyl chain is in a vertical orientation; this discrepancy is probably caused by crowding of the emerging PVP/C_{10}I chains, leading to some residues adopting an edge-on conformation. Kawaguchi and co-workers[20] have shown that the alkyl groups associated with relatively short P(4-VP_n/RBr) (n = 20–80) polyelectrolyte chains proceed from a prone to a vertical orientation in a broad, first-order transition with π_t = 0.25 mN/m (R = n-C_{12}) and 1.5 mN/m (R = n-C_8). This first-order transition at very small π values is observed over the 5–50 nm²/VP range. Our diblock samples, on the other hand, exhibit no measurable surface pressure in this area region, suggesting that the crowding caused by the self-assembly process forces the C_{10} chains into the air phase in the case of starfish surface micelles. This, plus the fact

Table II
Measured Values for Surface Micelles of P(S_{260}-b-VP_n/C_{10}I) at 2 mN/m

	n = 13	n = 29	n = 71	n = 120	n = 240
morphology	plane	rod	starfish	starfish	starfish
D (nm)[a]	43–420	47 ± 2	42 ± 6	37 ± 5	34 ± 5
d (nm)[b]		80 ± 3	82 ± 13	95 ± 12	125 ± 28
r (nm)[c]		16 ± 2	20 ± 6	29 ± 8	45 ± 17
h (nm)[d]	5.5–9		9.3 ● 1.2	7.1 ± 1.0	7.6 ● 1.5
			N_{Agg}		
method[e]	n = 13	n = 29	n = 71	n = 120	n = 240
total area			183 ± 1	124 ± 6	122 ± 3
individual micelle area			176 ± 47	159 ± 48	131 ± 35
hexagonal lattice			200	134	131
PS volume[f]	10^2–10^4	8[g]	213 ± 67	138 ± 41	125 ± 51
PS area	10^2–10^4		128 ± 33	97 ± 2	83 ± 2

[a] D = average diameter of PS cores for starfish micelles, average widths for rod micelles, and average diameters for planar aggregates. [b] d = average center-to-center distance between PS cores. [c] r = (d – D)/2; half the distance between edges of adjacent PS cores. [d] h = height or thickness of the PS cores measured by metal shadowing. [e] Methods of calculating N_{Agg} from TEM's. For details, see ref 7. [f] Using h_e = 4 nm (ref 7). [g] The aggregation number for rod micelles is unimers per nm.

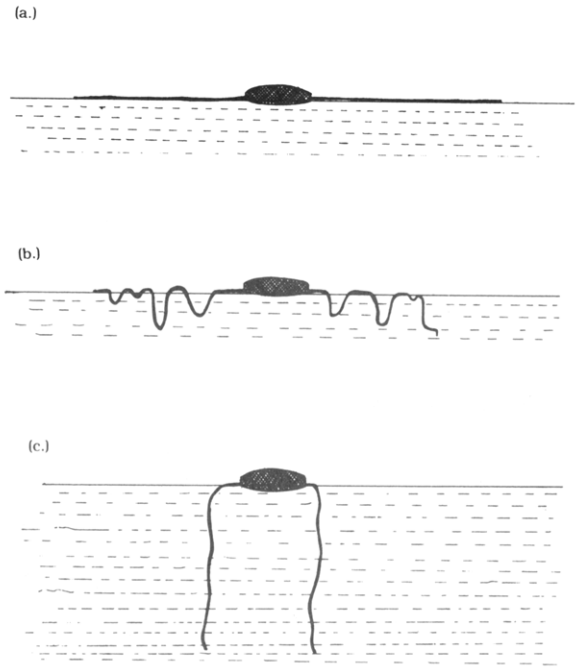

Figure 10. Schematic representation (side-on view) of a (a) starfish surface micelle, (b) a "partial" jellyfish surface micelle, and (c) a "complete" jellyfish surface micelle.

that the onset at A_{on} (Figure 2) is rather sudden, suggests that self-assembly of these molecules occurs at the air–water interface at $\pi = 0$ mN/m.

The onset of surface pressure at A_{on} arises from short-range interactions which initially occur between surface-absorbed VP's. An extensive series of LB films of monolayers deposited at low π (2 mN/m) and visualized by TEM show the halfed intercore distances to be ~20–45 nm (r in Table II). The theoretical, fully stretched length of the corresponding P(VP/C_{10}I) chains ranges from 18 to 60 nm. These values suggest that the surface-adsorbed P(VP_{240}/C_{10}I) chains are actually quite extended, especially near the core. The surface pressure at A_{on} is therefore believed to be due to repulsive interactions between surface-adsorbed polyelectrolyte chains in *adjacent* surface micelles. These interactions will have both steric and electrostatic components. Because virtually every repeat unit is ionized, the Debye length (in the absence of external electrolyte) will probably greatly exceed the repeat distance along the chain. This suggests that the chains should be highly extended. It should be borne in mind that there will be a substantial chain entropic contribution. A crossing of chains on the water surface is probably unlikely. Such a situation would be energetically costly as it would require one chain being submerged into the subphase while the other chain is being forced into the air phase.

The surface area contributed per PS block can be estimated in several ways. First, one can measure the total area of the PS cores of individual micelles and divide it by N_{Agg}; the N_{Agg} calculation technique employed cannot of course be the PS area method.[7] Second, A_2 (for starfish-forming molecules) can be plotted against the number of VP residues, n, and extrapolated to $n = 0$. Third, one can use Kumaki's empirical expression ($A_{PS} = 0.04MW$; ref 22) derived from PS homopolymer/film balance experiments to estimate the area per PS block. Table III lists the area values calculated for each PS block length using these methods. Of note are the PS core dimensions relative to the PS chain dimensions. For example, the P(S_{260}-*b*-VP_{240}/C_{10}I) core has a radius of ~17 nm. The corresponding fully stretched length of $(PS)_{260}$ is ~65 nm and the random coil dimension is ~10 nm. The radius of 17 nm suggests that the PS chains in the core are modestly extended compared with the random coil state.

Table III
Values of Area per PS (A_{PS}, nm²/PS) for P(S_m-*b*-VP_n/C_{10}I) Calculated Using Three Methods

M	$A_{PS\ core}/N_{Agg}$[a]	$A_2(n = 0)$	$0.04MW_{PS}$
54	*b*	2.4	2.2
180	6.4	6.8	7.5
260	7.2	0.8	10.8
480	12.2	16.2	20.0

[a] N_{Agg} was calculated using the individual micelle area method.[7] [b] No starfish micelles were observed for P(S_{54}-*b*-VP_n/C_{10}I) block copolymers.

The monotonic increase in surface pressure between A_{on} and the onset of the transition (A_1) corresponds to the interpenetration or lateral compression of surface-adsorbed, radially oriented chains of adjacent aggregates. The crowding caused by these processes can cause reorientation of the VP rings from a flat, surface-adsorbed configuration to an edge-on conformation. At A_1, all of the accessible free surface area is exhausted. The value of A_1 after subtraction of the PS areas ranges from 0.13 to 0.22 nm²/VP residue (Table IV). Once again, this is in the range predicted by molecular models—this time for edge-on, *n*-alkylated VP. Therefore, at A_1 the entire water surface is believed to be covered by aggregated PS plus interdigitated and compressed P(VP/C_{10}I) chains whose C_{10} moieties have assumed a vertical orientation.

Compression of each circular surface micelle past A_1 leads to a plateau in the isotherm. The plateau pressure, π_t, is independent of the length of the P(VP/C_{10}I) chain above ~80 residues (i.e., 35 mN/m), and for materials having between 10 and ~80 residues it increases monotonically from 29 to 35 mN/m. A_2 is the extrapolated end of the plateau, after which the isotherm exhibits a second region of relative incompressibility. An upward reorientation of the VP residues and their counterions into the air phase is energetically costly and therefore unlikely as a mechanism of the transition occurring at the plateau. Instead, a solubilization process occurs with minimal change in π throughout because of its incremental nature. Solubilization probably occurs via formation of VP loops attached to the surface via surface-adsorbed VP/C_{10} trains. Because A_2 values are larger than the size of the PS in the cores (i.e., $A_2 \approx 14$–36 nm²/molecule and the area per PS in the core is ≈11 nm²/PS), for P(S_{260}-*b*-VP_n/C_{10}I), the solubilization process is evidently incomplete at 25 °C and some VP residues remain surface adsorbed at A_2. Even when the surface pressure increases up to film collapse values, some P(VP/C_{10}) groups remain surface adsorbed. The surface micelle at A_2 thus resembles a "partial" jellyfish and not a "complete" jellyfish (Figure 10). Clearly, however, the block polyelectrolyte molecules proceed from a surface-adsorbed state at A_1 to a three-dimensional state at areas less than A_2. The A_2 values for example (accounting for the PS core areas) are equivalent to an area per VP residue of ~0.10–0.15 nm² for the $(PS)_{260}$ material. This small value requires that some "multilayering" of the PVP^+ chains has occurred. Complete solubilization of the decylated chain does not occur because the solubility limit of the P(VP/C_{10}I) chain in the aqueous subphase at the interface is reached and/or osmotic pressure effects become important.[23] The consistency of the data with a soluble loop/surface train description suggests that the solubilization process occurs randomly

Table IV
Calculation of Isotherm Values for $P(S_m\text{-}b\text{-}VP_n/C_{10})$

		A_{on}				A_1				A_2			
m	n	a	b	c	d	a	b	c	d	a	b	c	d
180	73	34	0.36	0.38		20	0.16	0.19		14	0.08	0.10	
180	190	85	0.41	0.41		45	0.19	0.20		26	0.09	0.10	
260	71	30	0.27	0.32	0.50	18	0.10	0.15	0.24	14	0.04	0.10	0.15
260	120	62	0.42	0.46	0.58	34	0.19	0.22	0.28	25	0.12	0.15	0.19
260	240	109	0.41	0.43	0.47	58	0.20	0.22	0.24	36	0.10	0.12	0.13
480	79	38	0.23	0.33		22	0.03	0.13		19	0.00	0.09	
480	200	77	0.28	0.32		43	0.11	0.15		31	0.06	0.09	
0	480	240	0.50			134	0.28			62	0.13		

[a] Measured area per molecule from π–A isotherms (nm^2/molecule). [b] Calculated area per VP residue (nm^2/VP) after subtracting $A_{PS} = 0.04MW_{PS}$;[22] A_{PS} = 8 nm^2 for $(PS)_{180}$, 11 nm^2 for $(PS)_{260}$, and 20 nm^2 for $(PS)_{480}$. [c] Calculated area per VP residue (nm^2/VP) after subtracting A_{PS} determined in Table III, using $A_{PS} = A_{PS\ core}/N_{Agg}$. [d] Area per VP residue (nm^2/VP) calculated by arbitrarily removing 25 VP residues from the total number of VP's. In this case, A_{PS} was taken from Table III ($A_{PS} = A_{PS\ core}/N_{Agg}$) and the number of effective VP's is considered to be 46, 95, and 215, respectively.

along the chain and not incrementally from the terminal VP/C_{10} residue inward toward the core. Furthermore, the LB films show that the first-order behavior arises from coexistence between surface-adsorbed and submerged $P(VP/C_{10}I)$ chains and does not arise from the coexistence between complete starfish and complete jellyfish micelles (Figure 10).

Compression up to the point of film collapse corresponds to compression of the "partial" jellyfish micelles. The high surface pressure achievable before collapse arises because of the strong interactions between the surface-tethered ionic $P(VP/C_{10})$ chains and the aqueous subphase. The temperature dependence of surface pressure plateaus has been used to quantify thermodynamic parameters of the transition in both low MW and polymer materials.[16-18] This protocol can be applied to the materials examined here and ΔS_t is positive in each case (Table I). This is consistent with the submersion mechanism because submersion involves transition from a relatively ordered, 2D state to a more disordered, quasi-2D state. From a phenomenological point of view, a decreasing plateau surface pressure on increasing the temperature is reasonable in that the VP/C_{10} residues will have increased aqueous solubility at elevated temperatures. The surface-adsorbed chains are therefore more likely to partition into the aqueous subphase as the temperature increases. Consistent with this trend in π_t is the trend in A_2, where A_2 decreases as temperature increases, suggesting that a greater extent of polyelectrolyte chain submersion has occured at high temperature. In short, as the temperature increases, the surface micelle becomes a more complete jellyfish at high compression.

Compression rate data further support the preceding description of the transition process. The isotherm is fully reversible up to A_1; 2-dimensional chain alignment and reorientation of VP residues (prone to edge-on) will be relatively low energy processes and should have rapid kinetics associated with them. Chain submersion is a higher energy process and is kinetically slow as evidenced by the substantial differences in π_t on going from a 30- to a 600-min film compression. The solubilization and chain reorganization processes produce reasonably stable, partially submerged polyelectrolyte chains which require time to return to their surface-adsorbed starfish state at expanded areas. The partial jellyfish finds the $P(VP/C_{10})$ chains in a situation similar to a polysoap with its associated stabilizing factors (decyl–decyl interactions, partial ionic cross-links, etc.).

Comparison of the decylated diblock with the decylated homo-P(VP) is interesting. As mentioned above, short-chain (n = 20–80) P(VP)'s, when alkylated with long-chain bromides, have a first-order transition at very low pressure and large areas per VP residue (5–50 nm^2).[20] The homopolymer material examined in the present study, $P(VP_{480}/C_{10}I)$, expresses no surface pressure at large areas but instead has A_{on}, π_t, A_1, and A_2 values qualitatively similar to the starfish-forming $P(S_{260}\text{-}b\text{-}VP_n/C_{10}I)$ materials (Table IV). These similarities suggest that the long $P(VP_{480}/C_{10}I)$ molecules may also self-assemble at 0 mN/m to form some type of domain on the water surface. The nature of these possible domains is presently unknown because the material does not offer sufficient contrast for electron microscopy visualization. The lack of a low-pressure phase transition and the similarity of the A_{on} value to the diblock systems means that packing in these domains is such that the C_{10} chains are vertically oriented, with the atactic VP residues surface adsorbed. The π–A data are also consistent with a compression sequence involving $P(VP/C_{10}I)$ surface reorientation and interpenetration, followed by solubilization of $P(VP/C_{10}I)$ loops, followed in turn by eventual compression of these loops.

Quantitative differences between the homopolymer and the diblock surface films are apparent (Table IV). In particular, the A_{on}, A_1, and A_2 values are smaller in the diblock systems than the homopolymer. This could arise for two reasons. First, it is possible that a small number of VP residues do not express themselves in the diblock isotherm because they are effectively immobilized between the water and styrene layers. In this regard, the $P(VP/C_{10}I)$ residues may act as classic interfacial compatibilizers. Arbitrarily removing 25 VP residues from the calculation which determines values the area per VP results in values similar to the homopolymer case as well as providing consistency between the $P(S_{260}\text{-}b\text{-}VP/C_{10}I)$ samples themselves (Table IV). Alternatively, the differences apparent in Table IV could arise from subtle differences in the compression-induced packing of homopolymer and diblock systems. Starfish aggregation imposes a radial geometry on the VP chains, forcing them to emerge near the circumference of the PS core. This aggregation-induced crowding may cause the VP's closest to the PS core to adopt an edge-on conformation prior to any external compression, thus reducing the effective value of A_{on} per VP. Alignment of the homopolymer chains would not impose these constraints on the VP/C_{10} residues. The net result would be larger A_{on} but similar A_1 values for the homopolymer compared to the diblock. A_{on} values are larger for the homopolymer, suggesting that the VP chains in homopolymer and diblock samples undergo very similar compressional behavior and that the origin of A_{on}, A_1, and A_2 is the same in the two types of materials. They do differ in the surface pressure plateau in that the ho-

mopolymer sample plateau spans ~7 mN/m while the diblock plateau is much flatter, spanning ≈1 mN/m. This difference probably arises from the differences in the manner in which radially oriented and nonoriented surface-adsorbed chains respond to the anisotropic compression of the experiment.

Rod and Planar Aggregates. TEM's (Figures 6–9) clearly show that rod or planar aggregates are the predominant morphologies for materials which show little or no plateauing in the high-pressure region. Moreover, in the A_{on} region of the isotherm, each of these samples exhibits a more gradual increase in pressure compared to samples which have been shown to adopt the starfish morphology.

Beginning our discussion with the rod-producing samples $P(S_{480}$-b-$VP_{34}/C_{10}I)$, $P(S_{260}$-b-$VP_{29}/C_{10}I)$, and $P(S_{180}$-b-$VP_{29}/C_{10}I)$, one can see that the rods have several structural features in common. In their LB films, there can be a moderate degree of alignment of unbranched rods. We do not as yet know whether this alignment is initiated by shear forces associated with film lifting or if this alignment occurs on the water surface during the film compression process itself. There is considerable uniformity in both the widths and inter-rod spacings (Table II). If the rods arise from the juxtaposition of two surface-adsorbed random coils, then the measured width (47 nm for $(PS)_{260}$) is considerably larger than twice the random coil dimensions (i.e., ~20 nm) and is about 36% the length of two fully extended PS chains (~130 nm). Clearly, the PS chains in a bilayer configuration will be extended. This is the case to a lesser extent for starfish micelles. This chain elongation evidently places the system at, or near, a free energy minimum despite the unfavorable elastic energy needed to stretch the chain. The rod–rod spacing (~33 nm) at 2 mN/m surface pressure for the $P(S_{260}$-b-$VP_{29}/C_{10}I)$ material, on the other hand, is about twice the combined length of the two PVP chains (~14 nm) if they are fully extended from the edge of the polystyrene rod.

The π–A curves show that little or no phase transition is found in rod-producing samples. Those samples that do show a small discontinuity also have starfish micelles present in their TEM's. Starfish–starfish interactions are believed to be the origin of the π_t in the corresponding isotherms. The absence of a transition in pure rod systems means that their very short VP chains do not manifest themselves in the measured π *if* they undergo a surface → subphase solubilization process upon compression. Compression of rods evidently does not lead to a plateau in an isotherm. The rods at low surface pressure are either randomly oriented on the water surface as individual rods or exist as domains of oriented rods. Starfish micelles, on the other hand, exist in a quasi-symmetric lattice even at π = 2 mN/m (Figures 6–9).

It is interesting to note that the A_2 values are dependent upon the P(VP) length. For example, A_2 for $P(S_{260}$-b-$VP_{13}/C_{10}I)$ = 6 nm²/molecule, $P(S_{260}$-b-$VP_{29}/C_{10}I)$ = 14 nm²/molecule, $P(S_{480}$-b-$VP_{13}/C_{10}I)$ = 9 nm²/molecule, and $(PS)_{480}(PVP/C_{10}I)_{34}$ = 17 nm²/molecule. The $P(VP/C_{10}I)$ chains associated with the rods apparently act as a nonpenetrable two-dimensional brush or comb. Once the rods reach close-approach distances, reorientation becomes energetically expensive and is therefore unfavorable.

Less readily defined than starfish or rod surface micelles, but no less interesting, are large planar micelles. These aggregates have a broad size distribution ($D \approx 40$ to $>10^3$ nm) and adopt a circular morphology in many cases. The circular morphology suggests that they have achieved an equilibrium state as it would represent a minimization of PS–water interactions along the circumference. Most aggregates have radii much greater than a fully stretched PS chain, allowing one to conclude that the planar, pancake-like surface micelles consist of a uniform polystyrene layer adsorbed onto the water surface with an intervening $P(VP/C_{10}I)$ layer. The height of large ($D >$ 100 nm) planar micelles is remarkably uniform (~6 nm) and corresponds to the dimensions of the appropriate PS random coil. The planar aggregates therefore appear to be a PS monolayer which is one molecule thick and hundreds of molecules wide. Interestingly, when homo-PS molecules are spread from a dilute solution and studied as LB films, they do not coalesce to form the coherent films seen in Figures 6–9 for the block copolymers.[22] Instead, they form individual spheres and appear to only clump together upon compression.

Small planar micelles ($D <$ 100 nm) are thicker than the large planar micelles. This is immediately recognizable from the differences in the TEM shadows for small and large surface micelles (Figures 6–9). Thicknesses > 6 nm suggest that the PS blocks either elongate beyond their random coil configuration or overlap in haystack fashion. In large aggregates, the area per PS exposed to water is adequately balanced by the $PVP/C_{10}I$ block to which it is attached. If a smaller aggregate is formed during the initial solvent evaporation, then the diblocks at the circumference comprise a significant proportion of the total number of unimers in the aggregate. These circumference-localized diblocks can, however, adopt a conformation where the $P(VP/C_{10}I)$ chain emerges equatorially and is surface adsorbed. In doing so, the PS block loses some of its amphiphilic intermediary and is exposed to larger quantities of interfacial water. Chain elongation serves to minimize the resulting unfavorable water–PS interactions, and the resulting surface micelle is thicker than random coil dimensions.

Finally, it is of interest to compare the block polyelectrolyte systems studied here with the polymers studied to date in monolayer/LB film work. It has been shown that good-quality, defect-free, LB films can be produced from polymers with a stiff backbone.[11] Because the monolayers described here are self-assembled structures made up of relatively small units, surface reorganization processes are kinetically accessible relative to those for high molecular weight materials. Furthermore, simple manipulation of the material's composition leads to a highly predictable and very interesting series of morphologies. As far as we are aware, polymeric materials tend to yield only thin, highly extended films.

Summary

A comprehensive Langmuir film balance/Langmuir–Blodgett film (electron microscopy) study of the novel surface aggregating behavior of the block polyelectrolytes $P(S_m$-b-$VP/C_{10}I)$ has been carried out. Through a detailed structure/property approach, we have shown that surface aggregates can assume at least three different morphologies and that one of these (starfish) has associated with it a compression-induced reorientation. We ascribe this transition to a reorientation of a surface-adsorbed $PVP/C_{10}I$ state to a subphase-solubilized state. A detailed analysis of this transition is presented in a subsequent paper.[15] These studies further show that diblock polyelectrolytes self-associate in two dimensions into what are believed to be novel 2D surface micelles of various morphologies. Further aspects of the interfacial chemistry of these materials are the subject of study in our laboratories at the present time.

Acknowledgment. Financial support of this research from NSERC (Canada) to R.B.L. and A.E. is gratefully acknowledged.

References and Notes

(1) Zhu, J.; Eisenberg, A.; Lennox, R. B. *J. Am. Chem. Soc.* **1991**, *113*, 5583.
(2) Tanford, C. *The Hydrophobic Effect*, 2nd ed.; Wiley: New York, 1980.
(3) *Encyclopedia of Polymer Science and Engineering*; Kroschwitz, J. I., Ed.; Wiley-Interscience: New York, 1985; Vol. 2.
(4) *Polymer Blends*; Paul, D. R., Newman, S., Eds.; Academic Press: New York, 1978.
(5) Thomas, E. L.; Anderson, D. M.; Henkee, C. S.; Hoffman, D. *Nature* **1988**, *334*, 598.
(6) (a) Gouin, J. P.; Williams, C. E.; Eisenberg, A. *Macromolecules* **1989**, *22*, 4573. (b) Feng, D.; Wilkes, G. L.; Leir, C. M.; Stark, J. E. *J. Macromol. Sci., Chem.* **1989**, *A26* (8), 1151. (c) Desjardins, A.; Eisenberg, A. *Macromolecules* **1991**, *24*, 5779. (d) Selb, J.; Gallot, Y. In *Developments in Block Copolymer—2*; Goodman, I., Ed.; Elsevier Applied Science: London, 1985; Chapter 2.
(7) Zhu, J.; Lennox, R. B.; Eisenberg, A. *Langmuir* **1991**, *7*, 1579.
(8) Zhu, J.; Eisenberg, A.; Lennox, R. B. *Makromol. Chem., Macromol. Symp.* **1992**, *53*, 211.
(9) Zhu, J.; Lennox, R. B.; Eisenberg, A. *J. Phys. Chem.* **1992**, *96*, 4727.
(10) (a) Ulman, A. *An Introduction to Ultrathin Organic Films*; Academic Press: New York, 1991. (b) Gaines, G. L. *Insoluble Monolayers at Liquid-Gas Interfaces*; Wiley-Interscience: New York, 1966.
(11) (a) Duda, G.; Schouten, A. J.; Arndt, T.; Lieser, G.; Schmidt, G. F.; Bubeck, C.; Wegner, G. *Thin Solid Films* **1988**, *159*, 221. (b) Sauer, B. B.; Yu, H.; Kim, M. W. *Langmuir* **1989**, *5*, 278. (c) Niwa, M.; Hayashi, T.; Higashi, N. *Langmuir* **1990**, *6*, 263.
(12) Li, S.; Hanley, S.; Khan, I.; Varshney, S. K.; Eisenberg, A.; Lennox, R. B., submitted to *Langmuir*.
(13) Conner, M.; Kudelka, I.; Regen, S. L. *Langmuir* **1991**, *7*, 982.
(14) Cha, X.; Yin, R.; Zhang, X.; Shen, J. *Macromolecules* **1991**, *24*, 4985.
(15) Zhu, J.; Eisenberg, A.; Lennox, R. B. *Macromolecules*, following paper in this issue.
(16) Biegajski, J. E.; Cadenhead, D. A.; Prasad, P. N. *Langmuir* **1988**, *4*, 689.
(17) Motamura, K. *Adv. Colloid Interface Sci.* **1980**, *12*, 1.
(18) Adamson, A. W. *Physical Chemistry of Surfaces*, 3rd ed.; Wiley: Toronto, 1976.
(19) Meier, D. J. In *Thermoplastic Elastomers*; Legge, N. G., Holden, G., Schroeder, H. E., Eds.; Hanser: New York, 1987; Chapter 11.
(20) Kawaguchi, M.; Itoh, S.; Takahashi, A. *Macromolecules* **1987**, *20*, 1052.
(21) Granick, S.; Kuzmenka, D. J.; Clarson, S. J.; Semlyen, J. A. *Langmuir* **1989**, *5*, 144.
(22) Kumaki, J. *Macromolecules* **1988**, *21*, 749.
(23) Granick, S.; Herz, J. *Macromolecules* **1985**, *18*, 460.
(24) (a) Israelachvili, J. N.; Marcelja, S.; Horn, R. G. *Q. Rev. Biophys.* **1980**, *13*, 121. (b) Mitchell, D. J.; Ninham, B. W. *J. Chem. Soc., Faraday Trans. 2* **1981**, *77*, 601.